Waste Management Bulletin 2 (2024) 1–15

Contents lists available at ScienceDirect

Waste Management Bulletin

journal homepage: www.elsevier.com/locate/wmb

Valorization of ladle furnace slag and functional enhancement of post-adsorption materials

Otmane Sarti [a,*], Emilia Otal [b], Fouad El Mansouri [c], Hajar Ghannam [d], Salaheddine Elmoutez [e], Mustapha El Hadri [f], Mohamed Saidi [a], José Morillo [b]

[a] Laboratory of LAMSE, Faculty of Sciences and Techniques of Tangier, P.O. Box 416, Tangier 90000, Morocco
[b] Department of Chemical and Environmental Engineering, University of Seville, Camino de los Descubrimientos, s/n., Seville 41092, Spain
[c] Research Team: Materials, Environment and Sustainable Development (MEDD), Faculty of Sciences and Techniques of Tangier, Abdelmalek Essaadi University, BP 416, Tangier, Morocco
[d] Université Abdelmalek Essaadi, FST Tanger, Laboratoire Couches Minces et Nanomatériaux (CMN), Tanger 90000, Morocco
[e] International Water Research Institute, Mohammed VI Polytechnic University, Lot 660, Hay Moulay Rachid Ben Guerir, 43150, Morocco
[f] Condensed Matter Physics Team, Faculty of Sciences, Abdelmalek Essaadi University, Tetouan, Morocco

ARTICLE INFO

Keywords:
Metallurgical slags
Adsorption-Carbonation
Pyrolysis
CO_2 sequestration
Wastewater treatment
Circular economy

ABSTRACT

Carbonating metallurgical slags plays a pivotal role in achieving efficient mineral CO_2 sequestration and waste valorization. This research introduces a novel integrated approach that combines the carbonation of Ladle Furnace Slag (LFS) with the simultaneous degradation of Methyl Orange (MO) in synthetic water. The comprehensive characterization of LFS was conducted using X-ray Diffraction (XRD), X-ray Fluorescence (XRF), Inductively Coupled Plasma Optical Emission Spectroscopy (ICP-OES), Brunauer-Emmett-Teller (BET) analysis, and Scanning Electron Microscopy (SEM). The adsorption experiments reveal the high LSF capacity for MO degradation (149.25 mg/g) following pseudo-second-order kinetics (R^2 = 0.99) and Langmuir isotherm (R^2 = 0.98). The adsorption process was primarily governed by chemical and electrostatic interactions. Analysis of LFS-loaded MO indicated a reduction in $Ca(OH)_2$ phases, responsible for CO_2 mineralization and the formation of calcite ($CaCO_3$). Furthermore, the study explored the reusability of LFS-MO composites through chemical and thermal modifications. Pyrolysis of carbonated LFS with KOH impregnation exhibited potential for regenerating $Ca(OH)_2$ phases, while thermal modification induced significant mineral and microstructural changes, creating new active sites at various temperatures. Additionally, the Fenton-like reaction followed by thermal modification resulted in a highly organized and microporous LFS structure with enhanced surface area and porosity. Moreover, modification with $ZnSO_4$ followed by thermal activation promoted the formation of ZnO nanoxides on the LFS surface. This research proposes an innovative carbonating approach for metallurgical slags and wastewater treatment, extending their utility and enhancing industrial sustainability. Carbonated LFS-MO composites hold promise for applications in construction, CO_2 capture, and wastewater treatment, thereby fostering sustainable industrial practices with ongoing research and development efforts.

Introduction

Diverse industrial activities, such as steel manufacture, foundries, blast furnaces, and biomass power plants, generate diverse types of residual byproducts. Unfortunately, these byproducts often end up in landfills, creating serious environmental issues and hindering circular economy concepts. Metallurgical slags contain high amounts of metal oxides like Fe_2O_3, Al_2O_3, MgO, and CaO, which show strong catalytic activity and are potential resources for wastewater treatment due to their large specific surface area that promotes pollutant adsorption (Ji et al., 2022; Rađenović et al., 2013).

Several studies have explored the use of slags in environmental applications. For instance, Basic Oxygen Furnace Slag (BOFS) has been used effectively for the degradation of petroleum hydrocarbons and the removal of dissolved organic carbon (DOC) and phosphate (Cha et al., 2006; Kim et al., 2021; Tsai and Kao, 2009). Steel slags have also been tested for enhancing soil carbon stability and mitigating CO_2 emissions (Wang et al., 2020). Thermally modified steel slag has shown higher

* Corresponding author.
E-mail address: otmane.sarti@etu.uae.ac.ma (O. Sarti).

https://doi.org/10.1016/j.wmb.2024.08.004

Available online 21 August 2024

capacity for removing organic matter, nitrate, ammonia, and phosphate from domestic wastewater (Wang et al., 2021a).

Ladle Furnace Slag (LFS), a byproduct of steel industry formed during the secondary refining, is produced in smaller amounts compared to other steel slags and has a distinct chemical composition with negligible ferrous oxides and increased fineness (Liu and Wang, 2017; Naidu et al., 2020; Yi et al., 2012). Despite its lower production volume, LFS has potential environmental applications, particularly in wastewater treatment. Additionally, the limited solubility of its mineral phases also results in a minor environmental impact (Rađenović et al., 2013; Sarti et al., 2023).

Treating steel slag with CO_2 before use is also a possible process known as carbonation. This procedure helps the free-CaO and MgO components to react with CO_2, leading to the creation of thermodynamically stable carbonates. This procedure enhances the mechanical durability of cementitious materials that include carbonated steel slag (Dong et al., 2021; Gomari et al., 2024; Huijgen and Comans, 2006; Jiang et al., 2018). Carbonation treatment is recognized for permanent carbon sequestration and waste valorization (Fang et al., 2024; Huang et al., 2024; Zhang et al., 2024).

Synthetic organic dyes are the most common variety of coloring substances, with over 100,000 commercially available varieties and a total yearly output volume exceeding 1,000,000 tons globally (Ali, 2010; Arora, 2014). Industries such as textile, tanning, printing, and paper heavily rely on these substances. Dyes represent a major and underrated group of contaminants within the aquatic environment due to their persistence, photochemical stability, and resilience against biological and chemical influences (Nidheesh et al., 2018; Suteu and Bilba, 2005; Tkaczyk et al., 2020). Certain dye compounds have been revealed to induce carcinogenic, allergic, and dermatological effects (Chung, 2016; Dutta et al., 2024). The consumption of water contaminated with textile dyes can harm human and animal health owing to their toxicity and mutagenicity (Haque et al., 2021; Kishor et al., 2021; Maruthanayagam et al., 2020).

The primary objective of this study is to valorize Ladle Furnace Slag (LFS), an industrial byproduct, by demonstrating its capability to remove the organic dye Methyl Orange (MO) from wastewater. This process not only removes the dye but also results in the carbonation of LFS, offering a dual advantage. Initially, LFS is characterized using advanced techniques such as XRD, XRF, ICP-OES, BET analysis, and SEM. Following this characterization, the adsorption dynamics of MO onto LFS are investigated through kinetic, isothermal, and thermodynamic analyses. Subsequently, a comparison between carbonated LFS and its raw counterparts is conducted to elucidate the mechanisms of both adsorption and carbonation processes. Furthermore, the study explores the reusability potential of carbonated LFS-MO composites through chemical and thermal modifications, including chemical impregnation with potassium hydroxide (KOH) followed by pyrolysis, thermal calcination at varying temperatures, and treatment with zinc sulfate ($ZnSO_4$). These treatments aim to modify the surface chemistry, morphology, and structural composition of LFS to optimize its performance in applications such as wastewater treatment and CO_2 sequestration, thereby contributing to sustainable industrial practices. Structural and morphological changes resulting from these treatments are examined using XRD and SEM. This research introduces an innovative approach to utilizing industrial byproducts for wastewater treatment, enhancing their utility and sustainability. The potential applications of carbonated LFS-MO composites extend to construction materials, CO_2 sequestration, and the development of efficient materials for wastewater treatment, supporting a circular economy and sustainable resource utilization.

Material and methods

Sample collection and preparation

The LFS under investigation was sampled from a metallurgical company located in Alcalá de Guadaíra (Seville, Spain). The samples underwent sieving at 200 μm, and no further modifications were made. Characterization of the material was conducted both before and after adsorption, as well as following reagent and thermal modifications.

Sample characterization

The pH measurement of the LFS sample was conducted according to the 9045D method using a pH meter Thermo Fisher Scientific, Waltham, MA, USA. The major and trace elements in the LFS were determined using an inductively coupled plasma–optical emission spectroscopy (ICP/OES) (Agilent 5100 model from Tokyo, Japan). Prior to analysis, the studied samples were digested using a mixture of nitric acid (HNO_3) and hydrochloric acid (HCl) in a 1:3 (v/v). Afterward, the pore size distribution, specific surface area, and nitrogen adsorption–desorption curve of LFS, were investigated using Brunauer–Emmett–Teller (BET) and Barrett-Joyner-Halenda (BJH) analysis using a BET Surface Area Analyzer (Micromeritics Tristar II 3020, Norcross, GA, USA).

For the examination of the structural and morphological characteristics of the LFS samples, scanning electron microscopy (SEM) was employed (FlexSEM 1000, Hitachi, Tokyo, Japan). Concurrently, the elemental composition of the LFS was determined using X-ray fluorescence spectrometry (XRF) with a PANalytical Axios FAST simultaneous WDXRF instrument (Almelo, The Netherlands). The crystalline composition of the LFS was analyzed using an X-ray diffractometer (Bruker D8A25, Bruker Corporation, Karlsruhe, Germany).

In order to study the reusability of LFS after the adsorption experiments the solid material was recuperated through centrifugation followed by filtration and wet samples were dried at 105 °C to remove excess of water. To study the carbonation process during adsorption, the LFS was characterized using XRD and SEM. In addition, thermal and chemical modification was performed to ensure a better reutilization of LFS adsorbate particles. The next step consisted of the calcination of carbonated LFS under different temperatures (300 °C; 500 °C. 1000 °C). Subsequently, the LFS adsorbate particles were mixed with KOH (1:1 ratio) and pyrolyzed under N2 flux to study the regeneration process. In this context, Carbonated LFS was introduced in a stainless-steel tube under nitrogen flow of 100 mL/min for 2 h at 700 °C. Lastly, carbonated LFS was treated using H_2O_2 (35 %) and ferrous solution $FeSO_4$, and subsequent calcination at 1000 °C. Lastly, the carbonated LFS was mixed with a 1 M zinc sulfate ($ZnSO_4$) solution to explore the potential synthesis of zinc oxide (ZnO) particles-based LFS after calcination at 700 °C. The carbonated LFS serves as a precursor for the synthesis of ZnO nanoparticles, with zinc sulfate acting as a zinc source during the reaction. The mixture was subjected to calcination at 700 °C, a temperature chosen to facilitate the conversion of the precursor material into the desired ZnO phase.

Batch adsorption studies

The adsorption of MO onto LFS was studied as a function of time, pH, initial concentration, adsorbent dose, and temperature. The experiments were carried out in closed glass flasks (batch) at room temperature. The solid–liquid ratios used are 1 g/L. The mixture is stirred until equilibrium time is reached at a constant temperature ensured by an incubator. At the end of the adsorption, the suspensions are filtered by non-sterile cellulose acetate syringe filters with a diameter of 30 mm and a porosity of 0.45 μm.

The residual concentration of MO was measured by UV-V double beam at 465 nm using Jasco 630 spectrophotometer (JASCO Corp., Tokyo, Japan). The quantity (q_t) adsorbed is given by the following

Table 1
Physicochemical characterization of the LFS carried out by ICP-OES.

	pH	Ca %	As	Co	Cd	Cu	Hg	Ni	Pb	Zn	LoI %
LFS	12.65	15.11	N.D*	0.53	0.91	40.5	N.D*	17.0	24.56	320.3	15.11

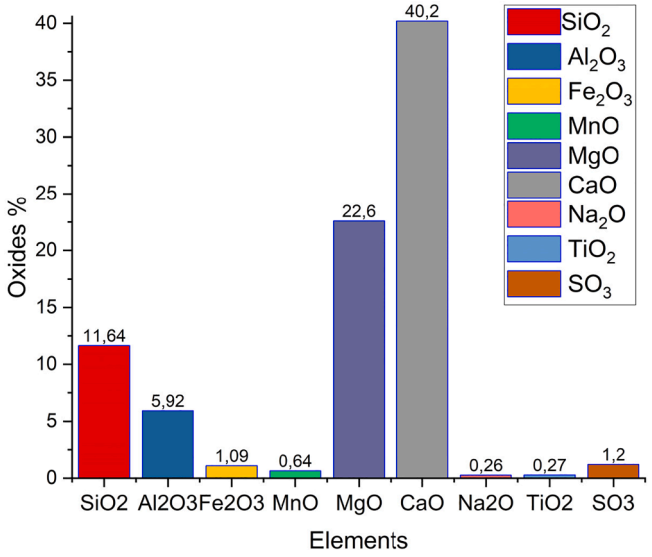

Fig. 1. Elemental composition of LFS by XRF.

relationship:

$$q_t = (C_0 - C_t) \times \frac{V}{m}$$

With:

q_t: quantity of MO per gram of adsorbent (mg. L^{-1});
C_0: initial concentration of the adsorbate solution (mg. L^{-1});
C_t: residual concentration at time t (mg. L^{-1});
V: volume of the solution (L); m: mass of the adsorbent (g).

Results and discussion

Physicochemical characterization

The Table 1 and Fig. 1 provide a comprehensive analysis of the physicochemical properties of LFS. Notably, LFS has a high pH principally attributable to the dissociation of intrinsic basic oxides upon contact with water. Through the process of hydrolysis, these oxides release alkaline molecules, therefore increasing the pH of the solution. Trace element analysis in the LFS decreased in sequence of Zn > Cu > Pb > Ni > Cd > Co, while As and Hg were not detected in the analyzed samples. Ecotoxicity tests have definitively shown that this substance is a nonhazardous industrial waste, confirming its safety and environmental suitability (Borges Marinho et al., 2017; Rađenović et al., 2013). The calcium showed a high content representing a considerable fraction of LFS. The X-ray fluorescence analysis confirmed that CaO was the dominant oxide exhibiting 40.2 % of the total LFS fraction. The LFS analyzed sample comprises a relatively higher amount of MgO, SiO_2, and Al_2O_3, exhibiting 22.6, 11.64, and 5.92 %, respectively. The XRF analysis showed also a minor presence of oxide such Fe_2O_3, MnO, TiO_2, Na_2O, SO_3 with a total percentage that not surpass 3.5 %.

*Non-detected.

XRD characterization of LFS

The Fig. 2 depicts the mineralogical composition of LFS. According to the XRD pattern, calcium silicate appeared as the predominant component in LFS, which comprises a variety of amorphous phases such as Calcium aluminum silicate hydrate or Katoite ($Ca_3Al_2(SiO_4)(OH)_8$), Calcium Silicate (Ca_2SiO_4), Calcium Hydroxide or Portlandite ($Ca(OH)_2$), and Calcium Silicate Hydrate ($3CaO{\cdot}2SiO_2{\cdot}3H_2O$). Additionally, there is a noticeable presence of Magnesium Hydroxide ($Mg(OH)_2$) peaks. The XRD analysis results for the examined LFS are consistent with previously reported findings (Rovnushkin et al., 2005; Setién et al., 2009; Yildirim and Prezzi, 2011) highlighting that Calcium silicates, in different allotropic forms, are the main constituents in the LFS (Rađenović et al., 2013).

BET analysis of LFS

Fig. 3 illustrates the N_2 adsorption/desorption isotherm for LFS, along with the BJH pore width distribution. Three pore types, namely micropores (d < 2 nm), mesopores (2 nm < d < 50 nm), and macropores (d > 50 nm), are categorized based on their diameters (Angın et al., 2013). As evident in Fig. 3, the average pore diameter of LFS predominantly falls within the 2–50 nm range, with some exceeding 50 nm. This observation indicates the coexistence of mesopores and macropores within LFS. The N_2 adsorption/desorption isotherms provide further support for this conclusion. Specifically, LFS exhibits an IV type N_2

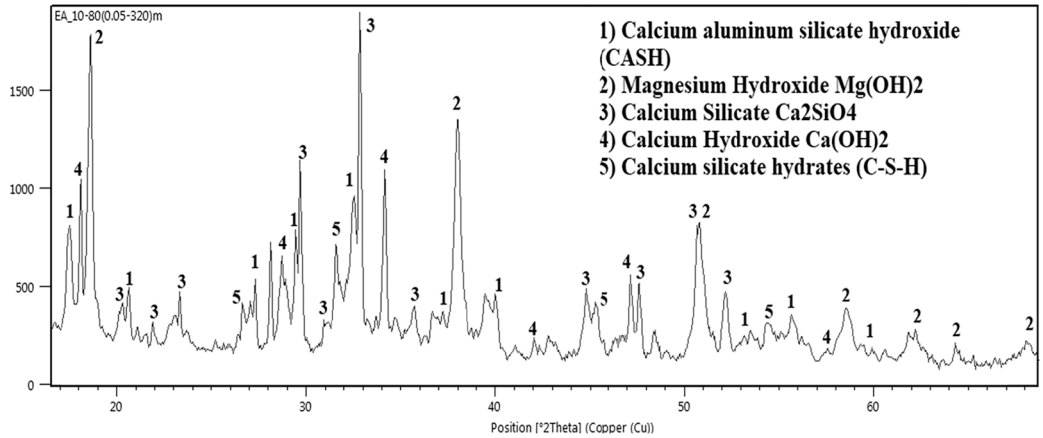

Fig. 2. XRD of Ladle Furnace Slag (LFS).

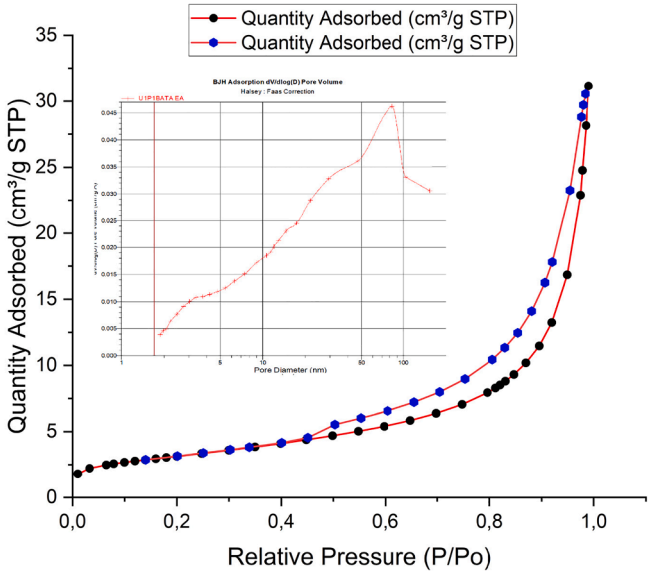

Fig. 3. BET Analysis of Ladle Furnace Slag (LFS).

adsorption isotherm with a pronounced hysteresis loop, indicative of mesopores. Additionally, the hysteresis loop extends towards an approach relative pressure ($P/P_0 = 1$), signifying the presence of macropores (Lin and Zhan, 2012). The BET analysis results reveal specific surface area (SSA), Langmuir Surface Area, average pore diameter, and pore volume values of 11.28 m^2/g, 15.61 m^2/g, 15.9 nm, and 0.049 cm^3/g, respectively. The chosen material, LFS, is distinguished by its significant surface area, rendering it highly efficient as an adsorbent. Beyond its chemical composition, the mesoporous structure of LFS imparts unique physisorption properties. In contrast, conventional metallurgical slags like steel slag, basic oxygen furnace slag, and Blast Furnace slags may exhibit limited surface characteristics. This distinction highlights the specific advantages of utilizing LFS in this study.

Morphological characterization of ladle Furnace slag (LFS)

Examining the raw Ladle Furnace Slag (LFS) using SEM shows a diverse structure with different oxides present in an amorphous state (Fig. 4). The micrographs display a complex matrix with irregular textures and morphologies, indicating the diverse composition of LFS. The amorphous nature of the observed phases suggests that the slag lacks long-range order and crystallinity, typical of glassy or non-crystalline materials. This heterogeneous structure is consistent with the diverse mineralogical composition of LFS, as indicated by XRD analysis, which identified phases such as $Ca(OH)_2$, $Mg(OH)_2$, Calcium Aluminum Silicate Hydroxide, Ca_2SiO_4, and Calcium Silicate Hydroxide Hydrate.

Adsorption of methyl orange (MO) on ladle furnace slag (LFS)

Adsorption Kinetics

The kinetics of MO adsorption onto LFS are depicted in the Fig. 5. Notably, the adsorption capacity of LFS concerning time is contingent on the initial concentration of MO. When MO concentrations are low (10–40 mg/L), the adsorption process is swiftly completed within 60–180 min, indicating rapid equilibrium attainment. In contrast, higher concentrations of MO result in a more prolonged adsorption period, occurring between 300 and 480 min. In simpler terms, the adsorption kinetics slow down due to the limited availability of active

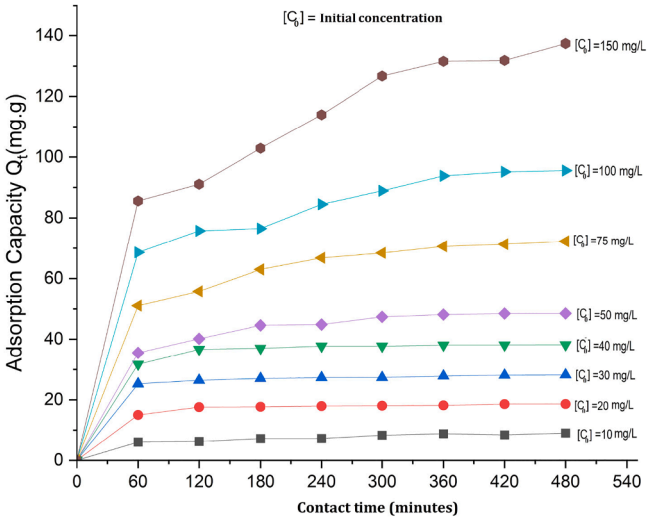

Fig. 5. Effect of contact time on MO degradation.

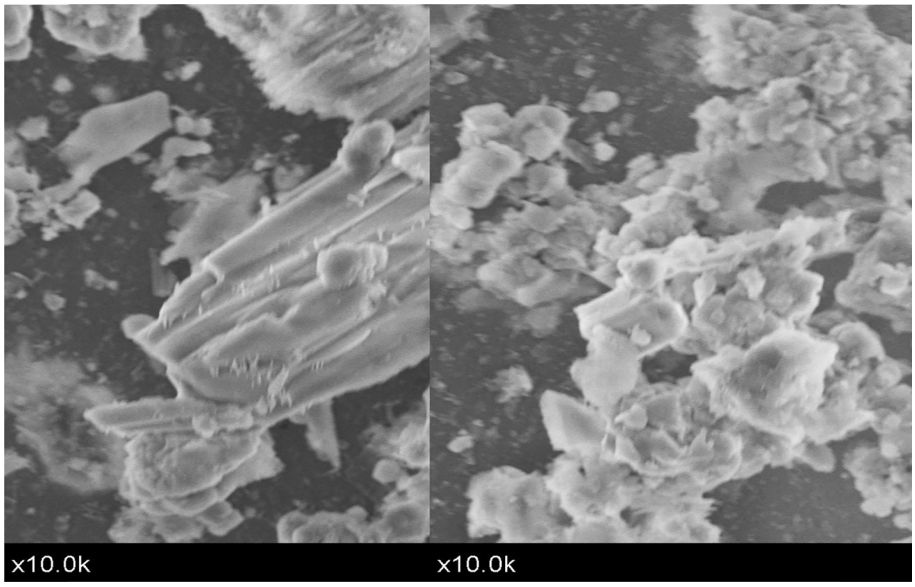

Fig. 4. Scanning Electron Micrograph (SEM) Revealing the microstructure of raw LFS.

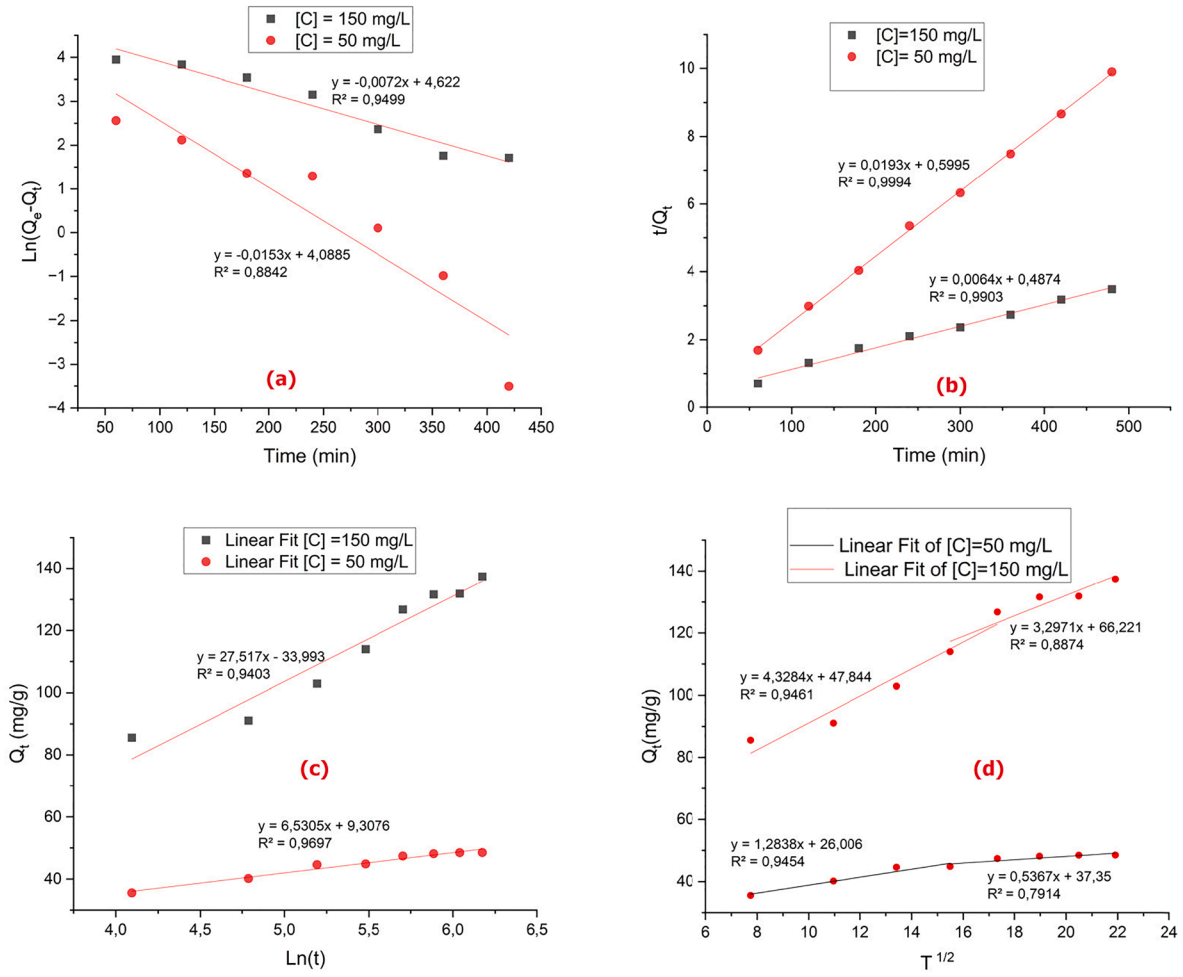

Fig. 6. Kinetic Behavior of MO Adsorption onto (LFS): (a) Pseudo-first-order, (b) Pseudo-second-order, (c) Elovich Kinetics, and (d) Intraparticle Diffusion Model. Experimental Conditions: Initial concentration of MO 50 mg/L and 150 mg/L; pH=6; T=293 K; Adsorbent dose 1 g/L; time = 420 min.

sites and the repulsive forces between the MO dye molecules already adsorbed on the LFS surface and those remaining in the solution. These repulsive interactions hinder the further diffusion of MO molecules into the internal pores of the adsorbent (Abdelaziz et al., 2023; Jebli et al., 2023). Regardless of removal mechanism it is admitted that the process MO degradation using LFS is influenced by diffusion and competition on the available LFS particles (El-Habacha et al., 2024; Lebkiri et al., 2023), for this reason higher concentrations such 100 and 150 mg/L require more time for achieving up to 90 % of MO elimination.

In order to investigate the processes controlling the time-dependent absorption of MO onto LFS, a variety of kinetic models were employed. The Pseudo-first-order Equation (1), Pseudo-second-order Equation (2), the Elovich Equation (3), and the Intra-particle models Equation (4).

Table 2
Outputs generated models from adsorption kenitics.

Models	Parameter	50 mg/L	150 mg/L
Pseudo-First-Order (PFO)	qe (mg/g)	59.65	101.70
	K_1 (min^{-1})	$-0.364.10^{-4}$	$-0.17.10^{-4}$
	R^2	0.8842	0.9499
Pseudo-Second-Order (PSO)	qe (mg/g)	51.81	156.25
	K_2 (g/mg.min)	0.00062	8.40378E-05
	R^2	0.994	0.99
Elovich	α (mg/g.min)	27.16	8.00
	β (g/mg)	0.15	0.036
	R^2	0.969	0.94
Intraparticle diffusion	C_1 (mg. g^{-1})	26.006	47.844
	C_2 (mg. g^{-1})	37.35	66.221
	$K1_{diff}$ ($g.mg^{-1}.min^{-1/2}$)	1.2838	4.3284
	$K2_{diff}$ ($g.mg^{-1}.min^{-1/2}$)	0.5367	3.2971
	R^2	0.9454	0.9461
	R'^2	0.7914	0.9974

$$\mathrm{Ln}(q_e - q_t) = lnq_e - K_1 \times t \quad (1)$$

qe = amount of dye adsorbed at equilibrium (mg/g)
qt = amount of dye adsorbed at time t (mg/g).
k1 = pseudo first order adsorption rate constant ($1.min^{-1}$).
t = time (min).

$$\frac{t}{q_t} = \left(\frac{1}{K_2 q_e^2}\right) + \frac{t}{q_e} \quad (2)$$

k2 = pseudo second order adsorption rate constant (g/mg.min).
qt = amount of MO adsorbed at time t (mg/g).
qe = amount of dye adsorbed at equilibrium (mg/g).
t = time (min)

$$q_t = \left(\frac{1}{\beta}\right) \times \ln(\alpha\beta) + \left(\frac{1}{\beta}\right)\ln(t) \quad (3)$$

qt is the sorption capacity at time t (mg. g^{-1}),
α is the initial sorption rate (mg. g^{-1} min^{-1}) and.
β is the desorption constant ($g.mg^{-1}$).

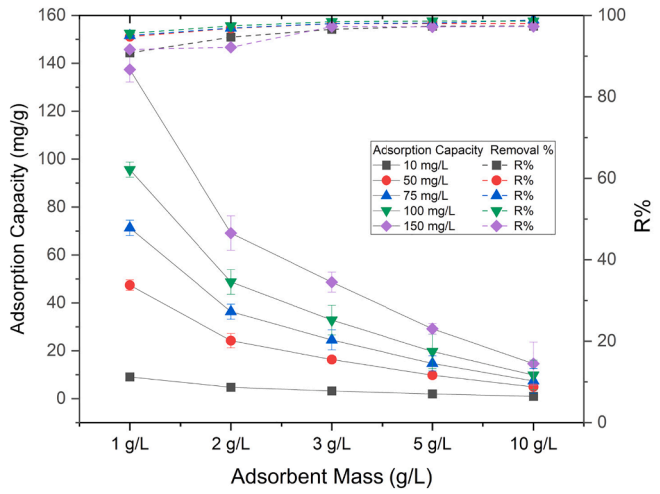

Fig. 7. Effect of LFS dose on MO degradation and adsorption capacity at different concentrations 10–150 mg/L.

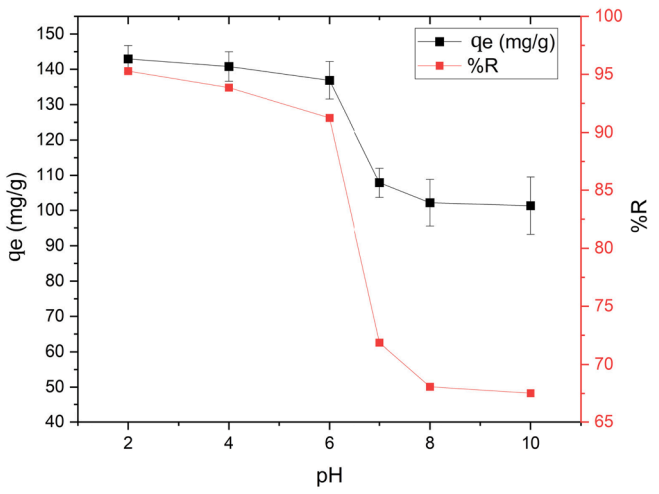

Fig. 8. Effect of pH solution on MO degradation. Initial concentration = 150 mg/L; Adsorbent dose 1 g/L; Time = 420 min.

In order to identify the diffusion mechanism, the kinetic results were analyzed using the intraparticle diffusion model. According to Webber and Morris, the kinetic expression of intraparticle diffusion is often presented by:

$$q_t = K_{int} \times \sqrt{t} + C \quad (4)$$

K_{int} is the constant of the rate ($g.mg^{-1}.min^{-1/2}$) and C is a constant of intra-particle diffusion model.

The Fig. 6 shows the fitting results of two experimental initial concentrations 50 and 150 mg/L according to the four investigated models. According to results (Table 2) The experimental data showed a relatively good correlation towards PFO kinetic model, (R^2 = 0.88) and (R^2 = 0.95), respectively. According to this model, the rate of adsorption is assumed to be directly proportional to the difference between the equilibrium and the instantaneous amounts of MO adsorbed on the LFS surface. While, the Pseudo-Second-Order model represented the most suitable adsorption kinetic model with a correlation $R^2 = 0.99$ for both investigated concentrations. This model assumes that the rate-limiting step of the adsorption process involves chemisorption, and it implies that the adsorption capacity is controlled by the availability of sites on the adsorbent surface. In addition, the model predicted a close result of the theoretical calculated qe of 51.8 and 156.25 mg/g, respectively.

Despite a lack of exact predictions regarding the adsorption process, the Elovich model is useful for describing adsorption on extremely heterogeneous adsorbents (Bulut et al., 2008). Notably, the model has a high correlation with the experimental data. The premise that chemisorption determines the rate of MO adsorption on the heterogeneous surface of LFS adds to its efficiency. As the concentration of MO increases, the parameter α decreases significantly, affecting the initial adsorption rate. Factors like the saturation of available adsorption sites or increased competition among MO molecules for accessible sites might explain this decline. As concentrations increase, β decreases, making desorption less effective. Stronger interactions between the MO molecules and the varied surface might explain the low desorption. This finding is consistent with the complex character of the heterogeneous surface, where differences in adsorption sites and affinities impact overall adsorption behavior.

The effect of LFS mass on the adsorption of MO

Determining the optimal adsorbent dose is essential for maximizing economic efficiency of decontamination mechanism. The presented Fig. 7 illustrates the adsorption capacity of LFS concerning both the adsorbent dose and initial concentration. The results reveals that an increase in adsorbent dose is associated with a decrease in efficiency, suggesting that smaller doses are sufficient to achieve equilibrium. Conversely, higher doses lead to improved removal efficiency, but at the cost of a sharp decrease in adsorption capacity. It is noteworthy that utilizing a minimal dose (1 g/L) while variying the initial concentration from 10 to 150 mg/L resulted in over 90 % removal of MO for each initial concentration. These reported results indicate that LFS dose does not affect clearly the adsoption rate of MO. Moreover, the removal efficiency remained relatively constant with varying adsorbent doses, suggesting that equilibrium is primarily influenced by the interaction between MO molecules and LFS surface. Despite the overall efficiency, the adsorption of MO onto LFS indicates a diminishing adsorption capacity. This signifies that smaller amounts of adsorbents are more effective in treating wastewater contaminated with MO dye. The observed trends highlight the intricate balance between adsorbent dose, removal efficiency, and adsorption capacity in optimizing the treatment process for MO-contaminated wastewater.

The effect of pH on MO adsorption onto LFS

The influence of pH on the adsorption of MO by LFS was investigated in this study. Fig. 8 shows that the adsorption of MO decreases with an increasing pH, while natural and acidic pH conditions result in greater removal efficiencies, reaching more than 90 %. This phenomenon is common in adsorption procedures where the pH of the solution significantly impacts the interaction between the adsorbate (dye molecules) and the adsorbent surface. At lower pH levels, the electrostatic attraction between the negatively charged dye molecules and the positively charged surface of LFS increases, promoting higher adsorption of MO (Baskaralingam et al., 2006). Under acidic conditions, the surface of LFS becomes positively charged, enhancing the interaction with the negatively charged MO molecules (Özcan and Özcan, 2004). This results in a more efficient removal process due to the increased electrostatic attraction. However, as pH increases, the surface charge of LFS changes, reducing the electrostatic attraction and thus the adsorption capacity. This decrease is attributed to the reduction in the number of protonated groups on the LFS surface and the increased competition from OH^- ions, which interfere with the binding of anionic dye molecules.

To overcome the pH effect and enhance the efficiency of MO removal, several strategies can be considered. As shown in this study, the adjustment of pH to a more acidic level before the adsorption process can help maintain a higher removal efficiency. This can be achieved also by adding acidic agents to lower the pH of the wastewater containing MO. Modifying the surface of LFS to introduce more positively charged functional groups can help maintain high adsorption capacities even at higher pH levels. Chemical treatments or acid activation of the LFS

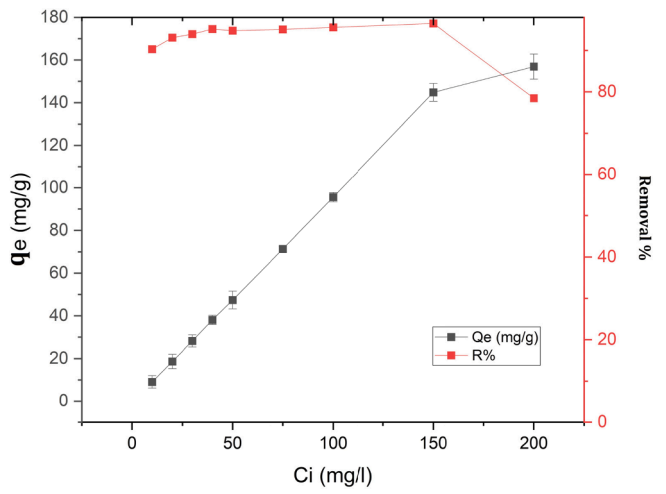

Fig. 9. Effect of initial concentration of MO on the adsorption capacity. Adsorbent dose 1 g/L; Time = 420 min; pH=6.

surface can be explored. Employing buffer systems to stabilize the pH during the adsorption process can help maintain optimal conditions for MO removal. This approach can prevent significant pH fluctuations that negatively impact adsorption efficiency. By implementing these strategies, the negative impact of increasing pH on the adsorption efficiency of MO can be mitigated, leading to more robust and effective wastewater treatment processes.

The effect of initial concentration on MO adsorption

In order to determine whether MO retention follows one or two models, or at most, the influence of initial MO concentration on the quantity adsorbed (mg/g) by the LFS throughout a range of initial concentrations from 10 to 200 mg/L was investigated (Fig. 9). A linear increase was observed in the adsorbed amount within the range of 10 to 150 mg/L suggesting that higher concentrations enhance the interaction between the dye molecules and the adsorbent surface (Loutfi et al., 2023). The ideal adsorption efficiency exceeded 90 % for each initial concentration. Nevertheless, a deviation from linearity occurred at the initial concentration of 200 mg/L. This variation demonstrated that 1 g/L of LFS concentration was inadequate to attain equilibrium for the higher MO concentration, implying that the interaction between MO molecules and the adsorbent had reached their maximum capacity. As a result, the percentage of MO removed decreased to 78.44 % when the concentration of MO was 200 mg/L. Overall, the experiment demonstrates that the adsorption of MO onto LFS is efficient when the concentration of MO is between 10 and 150 mg/L, and this relationship follows a linear pattern.

The Freundlich, Langmuir, and Temkin isotherm models were used to study the relationship between the amount of MO adsorbed onto the surface of LFS and the equilibrium concentration of MO in the solution. Linear equations for the Langmuir model Equation (5), the Freundlich model given by Equation (6), and Temkin Equation (7) were used in this study.

$$\frac{1}{q_e} = \frac{1}{K_l q_m} \times \frac{1}{C_e} + \frac{1}{q_m} \tag{5}$$

K_l illustrates the Langmuir constant ($L.mg^{-1}$), q max is the maximum

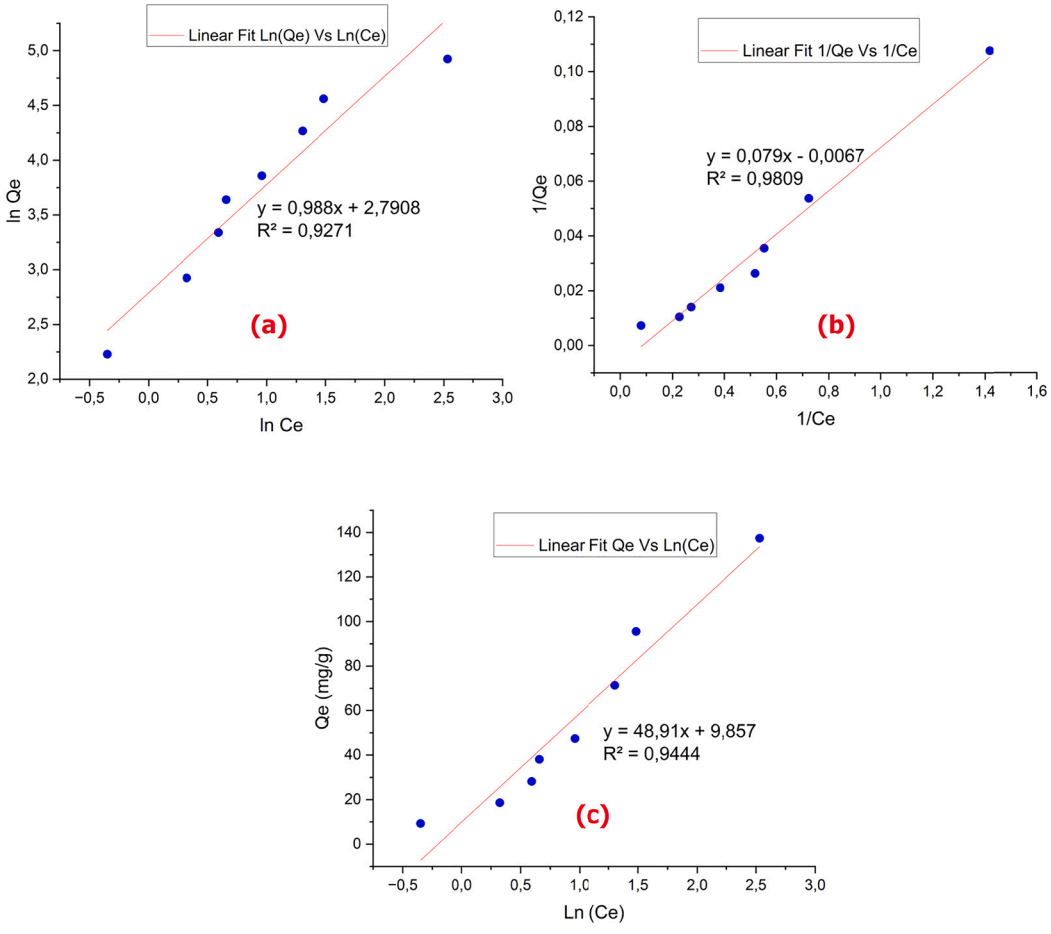

Fig. 10. Adsorption Isotherms of MO onto LFS: (a) Langmuir Model, (b) Freundlich Model, and (c) Temkin model.

Table 3
Isotherm parameters for the adsorption of MO onto LFS.

Isotherm	Freundlich			Langmuir				TEMKIN		
Parameters	R^2	Kf (mg/g)	nf	R^2	q_m (mg/g)	K_L (L.mg^{-1})	R_L	R^2	Bt (J.mol^{-1})	K_t (L.mg^{-1})
Value	0.92	16.29	0.72	0.98	149.25	0.08	0.54–0.072	0.94	48.91	0.72

adsorption capacity, and Ce is the equilibrium concentration in mg/L.

$$Log(q_e) = LogK_f + \frac{1}{n} \times Log(C_e) \quad (6)$$

Where, the Freundlich isotherm constant, K_f (mg/g), indicates the adsorption intensity in the equation, n is the Freundlich isotherm exponent, Ce indicates the adsorbate's equilibrium concentration (mg/L), and qe is the amount of MO adsorbed per gram of adsorbent at equilibrium.

$$q_e = \frac{RT}{b} + Ln(C_e) + \frac{RT}{b} + Ln(K_t) \quad (7)$$

where R, represent the gas constant (8.314 J/mol K), T absolute temperature (K), Ce adsorbate equilibrium concentration (mg/L), and b Constant related to heat of sorption (J/mol).

The isotherms for each of these models are depicted in Fig. 10, while the resulting parameters are tabulated in Table 3 for reference.

The obtained results clearly show that the adsorption of MO onto LFS is well described using the Langmuir model ($R^2 = 0.98$), followed by Temkin ($R^2 = 0.94$), and Freundlich ($R^2 = 0.92$).

The modelling according to Langmuir model demonstrates that the elimination of the MO by LFS takes place on a homogeneous surface according to monolayer adsorption without any interaction between the adsorbed ions with a maximum adsorption capacity q_{max} of 149.25 mg/g. The separation factor (R_L) shows whether the form of the isotherms is unfavorable (RL>1), linear (R_L=1), favorable (0 < R_L<1), or irreversible (R_L=0). The calculated R_L ranged between 0.54 and 0.072, indicating that adsorption of MO onto LFS is favorable. However, it is noteworthy that at higher concentrations, R_L approaches 0, suggesting that the MO concentration is sufficiently high to almost saturate the adsorption sites on the LFS surface. Consequently, further increases in concentration have a minimal impact on the adsorption process under these conditions.

Similarly, Temkin isotherm has showed a good correlation coefficient ($R^2 = 0{,}94$) suggesting a linear decrease in the heat of adsorption for all molecules inside a layer as coverage increases, ascribed to adsorbent-adsorbate interactions (Hu et al., 2018). Additionally, the adsorption is illustrated by a continuous distribution of bonding energies, attaining a maximum binding energy, as described by (Temkin, 1940).

Table 4
Thermodynamic parameters for MO adsorption on LFS.

Parameters	△G° (Kj.mol^{-1})				△H° (Kj. mol^{-1})	△S° (KJ^{-1} mol^{-1})
Temperature	298	308	318	328		
Value	−8.25	−4.73	−2.48	−1.78	−73.26	−220.18

The Freundlich model is applicable for heterogeneous surfaces because it allows for multilayer adsorption. The relatively good correlation of Freundlich model ($R^2 = 0{,}92$) suggests that MO molecules could form multiple chemical bonding on the LFS surface with varied affinities at distinct active sites, explaining the heterogeneity of LFS composition.

Lastly, it could be noted that the adsorption of MO onto LFS follows different mechanism including physisorption and chemical interaction between MO molecules and LFS mineralogical phases.

Thermodynamic study

To study the influence of temperature on the adsorption process of MO onto LFS, the same experimental protocol of the effect of the initial concentration ranging from 10 to 150 mg/l at the following temperatures: 25, 35, 45 and 55 °C was adopted. The suspensions were stirred at average speed using an incubator thermostat until reaching the equilibrium time. The results obtained show that the adsorption of MO by LFS decrease with increasing temperature. The thermodynamic parameters associated with the change in free energy (ΔG°), enthalpy (ΔH°), and entropy (ΔS°) could provide valuable insights into the thermodynamic adsorption behavior of MO on LFS. Thermodynamics parameters were calculated using the following equations:

$$K_d = \frac{q_e}{C_e}$$

$$LnK_d = \frac{\Delta S}{R} - \frac{\Delta H}{RT}$$

$$\Delta G = \Delta H - T\Delta S = -RTLnK_d$$

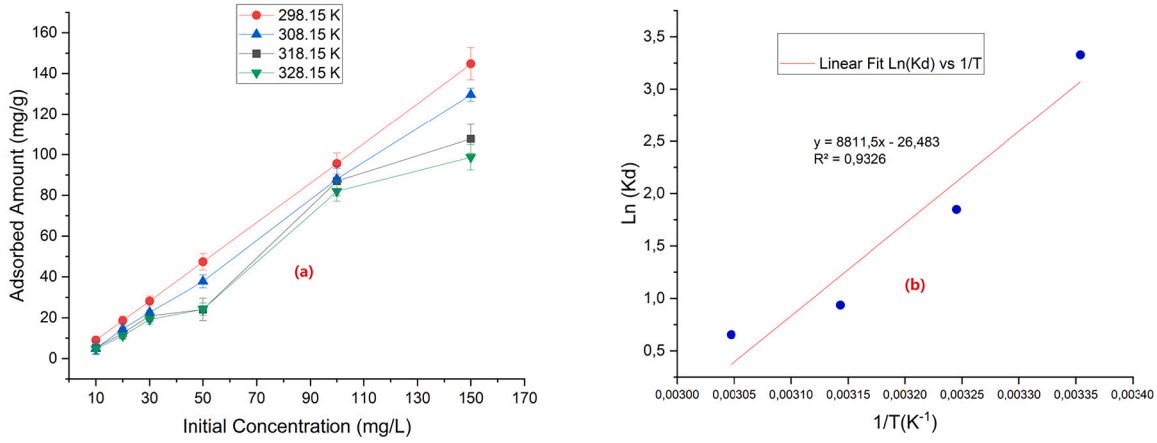

Fig. 11. Effect of temerature on MO adsorption (a) and adsorption thermodynamic (b).

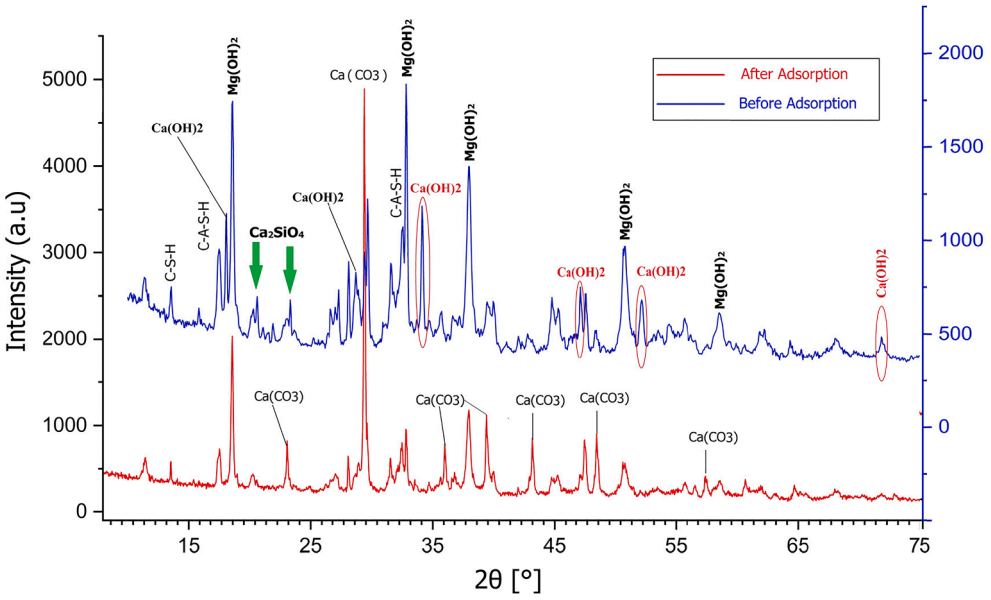

Fig. 12. XRD patterns of raw LFS before adsorption and LFS-MO after adsorption.

Where: Kd is the adsorption equilibrium constant, qe equilibrium adsorption capacity, C_e equilibrium concentration, and R is the gas constant (8.314 J.mol.K^{-1}). The parameters obtained from fitting Ln (Kd) versus 1/T (Fig. 11) are presented in Table 4.

The findings show a calculated enthalpy change (ΔH°) of −73.26 kJ/mol, indicating an exothermic adsorption mechanism between MO molecules and LFS. These MO molecules, which are present on the LFS surface and have accessible free sites, participate in adsorption via attractive forces, bond formation, or electrostatic interactions. As a result, this adsorption process releases energy in the form of heat, explaining the observed exothermic behavior. Furthermore, increasing the adsorption temperature causes the reaction to shift in the opposite direction, whilst decreasing the temperature allows for forward movement, hence improving the adsorption of MO molecules onto LFS. Furthermore, the entropy change (ΔS°) reveals a negative value of −220.18 KJ^{-1} mol^{-1}, indicating a reduction in the degree of randomness during MO adsorption on LFS. This negative entropy indicates a trend toward a more organized adsorption process. In other words, the system becomes less disordered, which is consistent with the exothermic character of the adsorption and indicates a preference for a more structured state during this molecular interaction.

Similarly, the free energy (ΔG°) exhibited a negatives values for the four investigated temperatures; The increase in (ΔG°) as temperature increases suggests that higher removal rates could be achieved in lower temperatures.

Mechanism of adsorption of MO onto LFS:

Fig. 12 depicts the characterization of Ladle Furnace Slag (LFS) before and after the adsorption of Methyl Orange (MO). The X-ray Diffraction (XRD) pattern displayed noticeable alterations post-adsorption, indicating the disappearance of certain phases from the LFS. Notably, Calcium Hydroxide vanished, while other peaks either remained unchanged or decreased in intensity, such as Calcium Silicate and Calcium Aluminum Silicate hydrate. Conversely, An obvious intense peak of calcite emerged in the LFS after adsorption, observed at 2θ = 29.40° attesting its better crystallinity (Wang et al., 2023). It should be noted that $Mg(OH)_2$ was identified after adsorption indicating less interaction with MO. While, the existence of $Mg(OH)_2$ could be explained by its low solubility in comparison with $Ca(OH)_2$.

Ladle Furnace Slag (LFS) exhibits a complex surface chemistry containing various functional groups, notably hydroxides (–OH) and metal oxides, including CaO, MgO, $Ca(OH)_2$, and $Mg(OH)_2$, as evidenced by XRD and XRF analysis. These metal oxides play pivotal roles in interacting with adsorbate molecules. MO molecules in aqueous solution reacts with LFS surface functional groups and metal oxides through multiple processes, such as electrostatic interactions between positively charged LFS surface groups and negatively charged MO molecules. Hydrogen bonding occurs between hydroxide groups on the LFS and functional groups on the MO molecules. The hydrolysis of LFS results in the release of hydroxide ions (OH^-), which interact with methyl orange molecules, facilitating the carbonation of the LFS surface and the formation of calcite $CaCO_3$. Furthermore, LFS could catalyze the oxidation of the azo (−N=N–) functional groups contained in MO, potentially leading to the fragmentation of the azo group and the production of smaller molecules. This cleavage could result in the breakdown of the MO molecule into simpler organic molecules or even inorganic substances such as CO_2. According to (Zavahir et al., 2023), with increasing reaction time, the degradation of MO led to the conversion of organic carbon components of the dye into CO_2, a transition identified through Total Organic Carbon (TOC) and Total Carbon (TC) analysis. This could explain that LFS due to its oxidizing agents facilitate the oxidation of organic carbon compounds. According to (Xu and Yi, 2022), carbonation treatment of LFS greatly improves heavy metal immobilization, CO_2 capture, and mechanical strength. Besides, Carbonated steel slag is projected to have less severe aquatic environmental repercussions than non-carbonated slag due to its lower alkalinity (Asaoka et al., 2013). In summary, Carbonated LFS may be used for a variety of applications, including CO_2 storage, improving concrete characteristics, and developing carbon dioxide-activated binders (Humbert and Castro-Gomes, 2019).

Post-Adsorption treatment (calcination, impregnation and pyrolysis):

The objective of the post-adsorption treatments explored in the following sections is to enhance the functional properties of Ladle Furnace Slag (LFS) following Methyl Orange (MO) adsorption and carbonation. This includes investigating chemical impregnation with potassium hydroxide (KOH) followed by pyrolysis, thermal calcination at varying temperatures, Fenton-like oxidation, and treatment with zinc sulfate ($ZnSO_4$). These treatments aim to modify the surface chemistry, morphology, and structural composition of LFS to optimize its performance in applications such as wastewater treatment and CO_2

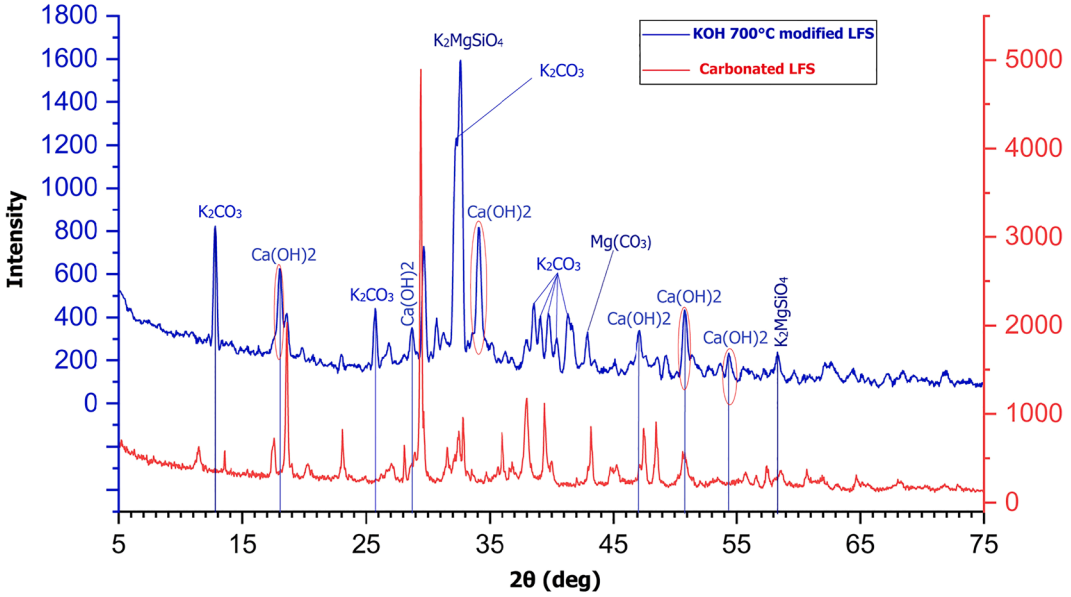

Fig. 13. XRD patterns of Carbonated LFS compared with KOH 700 °C modified LFS.

sequestration, thereby contributing to sustainable industrial practices.

KOH impregnation by pyrolysis

Composite modification is a method that involves blending one or more materials with steel slag in particular quantities, followed by high-temperature calcination or other modification techniques. This process, which is often used in the creation of composite-modified electrode slag particles, produces organic materials with improved catalytic performance and cost-effectiveness for electrical solutions (Z. Wang et al., 2021b; Zhang et al., 2020). In this study chemical impregnation of LFS-MO by potassium hydroxide KOH with a ratio of 1:1, followed by pyrolysis under N_2 gas at 700 °C was performed and the resulting XRD patterns are represented in Fig. 13.

The presence of nitrogen gas during pyrolysis influences the thermal stability of calcium silicate leading to their fusion while conserving oxygen containing groups in the form of (CO_3), and liberating (OH) to associate again with Ca forming thus Ca $(OH)_2$. $Ca(OH)_2$ conversions are estimated using XRD peak intensities from both original and thermally treated samples. As identified precedingly by XRD the $Ca(OH)_2$ phase which was reduced during the adsorption of MO was regenerated by KOH under pyrolysis indicating a substantial role of pyrolysis and KOH impregnation in regenerating $Ca(OH)_2$. It was also observed that Mg $(OH)_2$ peaks identified mainly at position similarly to (Albeladi et al., 2023; Saoud et al., 2014) were clearly reduced and replaced by $Mg(CO_3)$ and K_2MgSiO_4.

In addition, it was observed that calcium Silicate phases were also reduced leading to the formation of K_2MgSiO_4 at $2\theta = 32{,}57°$. According to (Ballotin et al., 2020), Serpentinite was subjected to chemical and thermal treatments using KOH to produce K_2MgSiO_4. These K^+ ions exhibit lower water solubility compared to typical potassium chloride (KCl), making them suitable for extended release of potassium fertilizer into soil.

$$CaCO_3 + 2KOH \rightarrow Ca(OH)_2 + K_2CO_3$$

Despite the conservation of Mg $(OH)_2$ phase after the adsorption, the pyrolysis caused a substitution of (OH) with CO_3, resulting in the regeneration of Ca $(OH)_2$ phases and $Mg(CO)_3$. Slags with low Ca concentration may have poor reactivity for CO_2 storage. Besides, the addition of K_2CO_3 may accelerate carbonation processes by creating more reactive sites for CO_2 absorption, increasing the slag's total CO_2 capture efficiency (Bejarano-Peña et al., 2021). In addition, CO_2 adsorption into promoted potassium carbonate solutions is a subject in carbon capture technology, especially post-combustion carbon capture from flue gases. Because of its strong CO_2 reactivity, potassium carbonate (K_2CO_3) is a popular chemical solution for CO_2 capture.

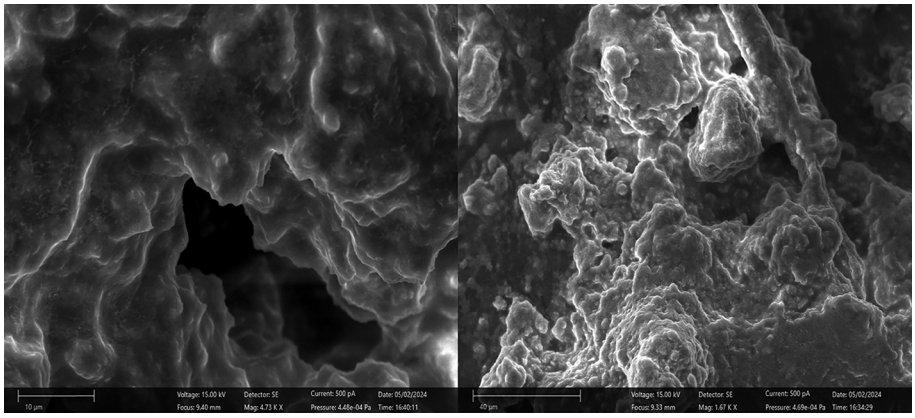

Fig. 14. SEM micrographs of carbonated LFS modified with KOH at 700 °C under pyrolysis.

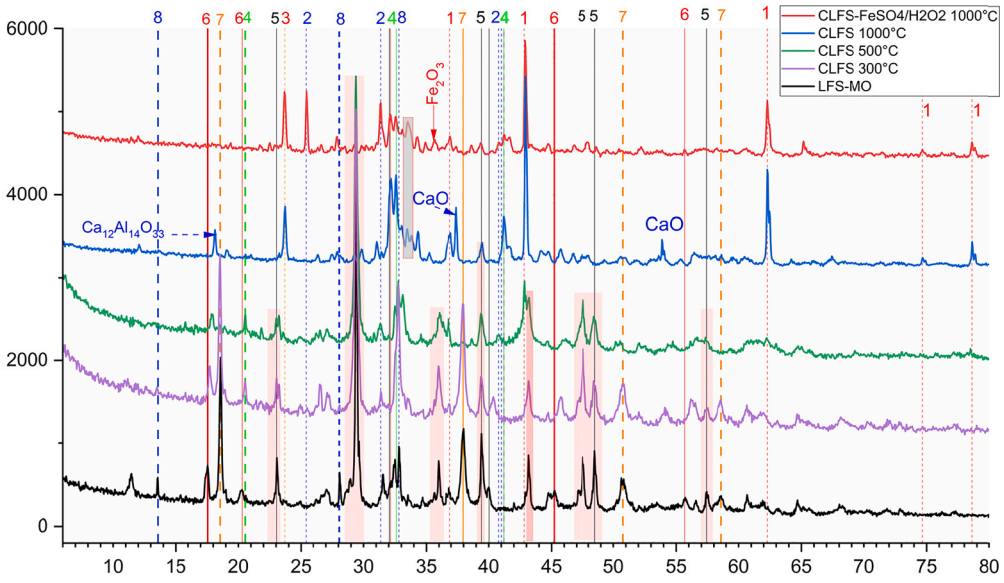

Fig. 15. XRD patterns of calcinated CLFS under different temperatures.

Table 5
Mineral phases of Carbonated LFS under different calcination temperatures.

ID peaks	Reference	Name	Chemical Formulae
1	01–078-0430	Periclase	MgO
2	01–072-0916	Anhydrite	Ca (SO_4)
3	00–042-1478	Calcium Sulfo-aluminate Sodalite	$Ca_4Al_6O_{12}SO_4$
4	00–033-0302	Larnite	Ca_2SiO_4
5	01–086-2334	Calcite	$Ca(CO_3)$
6	00–038-0368	Katoite, silication	$Ca_3Al_2(SiO_4)(OH)_8$
7	01–084-2163	Magnesium hydroxide	$Mg(OH)_2$
8	00–029-0330	Afwillite	$Ca_3(SiO_3OH)_2{\cdot}2H_2O$

$$Mg(OH)_2 + CaCO_3 \rightarrow Ca(OH)_2 + MgCO_3$$

$$Mg.SiO_2 + 2KOH \rightarrow K_2Mg(SiO)_2 + H_2O$$

According to SEM images (Fig. 14) the resulting KOH-LFS modified composite possesses a porous structure when compared with the raw LFS, this chemical and thermal modification improves the accessibility of active sites on the mineralized surface of LFS. This enhances the metal catalytic activity in a variety of chemical processes. The increased surface area enables more effective adsorption and reactivity of reactant molecules, resulting in improved catalytic performance. Accordingly, the pyrolysis process at different temperatures may potentially improve the distribution of pore diameters in activated carbon and its textural properties.

Effect of calcination on the carbonated LFS

Fig. 15 shows a comparative X-ray diffraction (XRD) analysis of carbonated Ladle Furnace Slag (LFS) derived from (MO) adsorption (designated as LFS-MO) in comparison to calcined LFS samples at temperatures of 300 °C, 500 °C, and 1000 °C, as well as carbonated LFS subjected to $FeSO_4/H_2O_2$ treatment at 1000 °C (denoted as CLFS-$FeSO_4$/H_2O_2 1000 °C). all the mineral phases detected are presented in Table 5.

The analysis revealed the presence of newly detected MgO phases, which are suggestive of RO phases, in three samples: CLFS-1000 °C, CLFS-500 °C, and CLFS-$FeSO_4$-H_2O_2 Simultaneously, a conspicuous decrease in the intensity of $Mg(OH)_2$ was observed in these samples, indicative of the dehydration of brucite. This phenomenon underscores the transformative effect of thermal treatment on the sample composition.

Furthermore, the heating process revealed distinct alterations in phase composition. Samples subjected to calcination at 1000 °C exhibited the disappearance of the Calcite phase, highlighting the temperature-dependent phase transitions. In contrast, CLFS-300 °C and CLFS-500 °C maintained consistent intensities of calcite such the carbonated LFS, indicating the preservation of the original phase constituents under milder thermal conditions.

Notably, the presence of CaO resulting from $CaCO_3$ decomposition was identified at $2\theta = 37.34°$ and $2\theta = 53.85°$. However, intriguingly, CLFS-$FeSO_4/H_2O_2$ treated at 1000 °C exhibited an absence of CaO peaks, suggesting the influence of the $FeSO_4$ solution. This observation hints at the substitution of the CaO phase with $CaSO_4$, further emphasizing the role of chemical treatments in phase evolution. Moreover, the association of Fe ions with oxygen from was facilitated by hydrogen peroxide, leading to the formation of Hematite (Fe_2O_3) at $2\theta = 35.64°$.

The heating process exhibited shifting and reduction in the intensity of Katoite $Ca_3Al_2(SiO_4)(OH)_8$ peaks mainly at positions 2θ = 17,56; 32,37; 39,91; and 45,21°. Under temperature effect this shifting caused the apparition of Mayenite $Ca_{12}Al_{14}O_{33}$ at samples CLFS 500 °C and 1000 °C. Synthetic katoite was found to be stable up to 275 °C, but according to (Eisinas et al., 2020), at higher temperature (350 °C), it undergoes complete recrystallization into mayenite. Between 850 and 1150 °C, the strength of mayenite-specific diffraction peaks increased significantly (Eisinas et al., 2019).

SEM images corresponding to the described XRD results are anticipated to depict microstructural variations reflective of phase transformations, compositional changes, and the influence of different thermal and chemical treatments on the studied samples, SEM images are depicted in Fig. 16. It was observed that carbonated LFS differs from the original LFS particles displaying rough surfaces, irregular shapes, and porous structures. In contrast, the SEM image of carbonated LFS (micrograph a) reveals a more compact structure and smoother surface compared to untreated LFS due to the filling of void spaces by calcite crystals. The presence of calcite crystals can be observed as distinct crystalline features on the surface and within the slag particles. Both

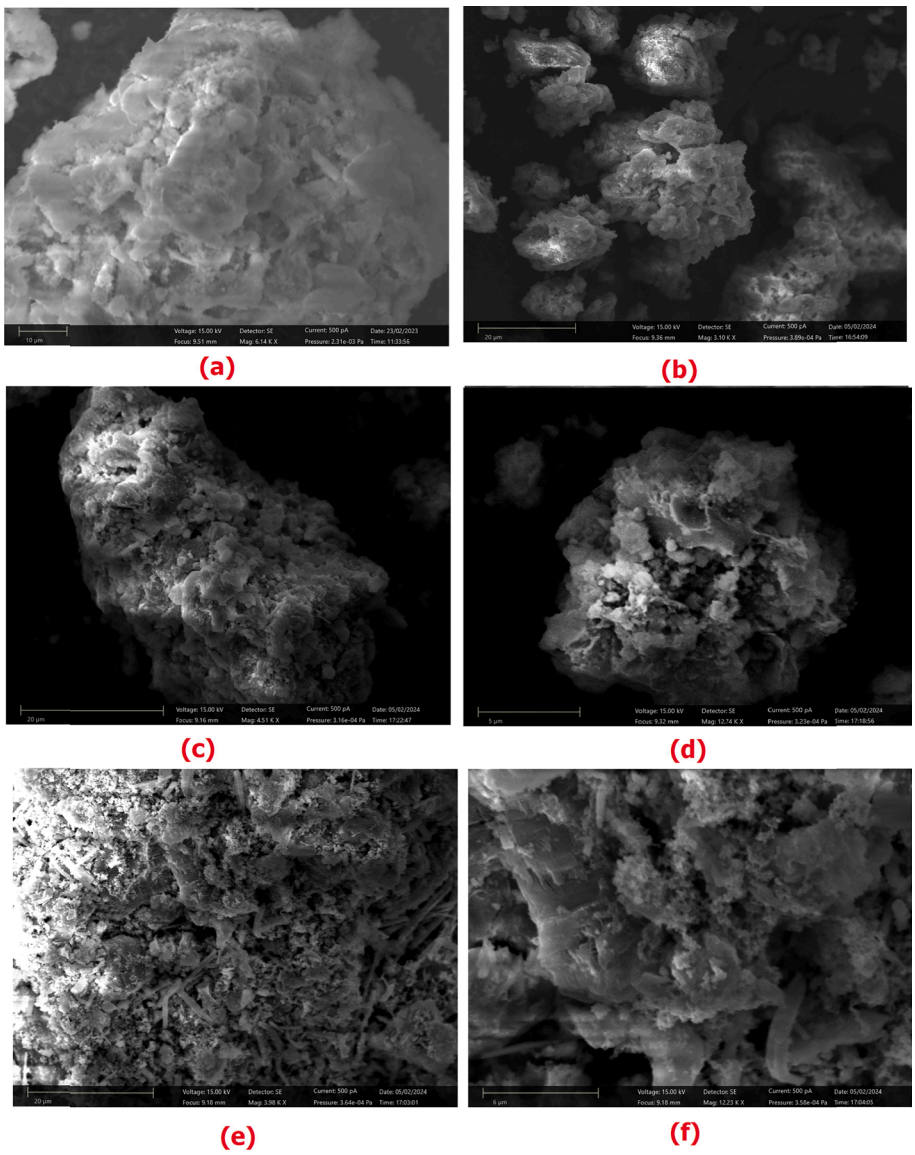

Fig. 16. SEM micrographs of (a) Carbonated LFS, (b) CLFS calcined at 300 °C, (c) CLFS calcined at 500 °C, (d) CLFS calcined at 1000 °C, and (e) and (f) CLFS treated $FeSO_4/H_2O_2$ at 1000 °C.

samples undergoing calcination at 300 and 500 °C did not reveal a major change in the morphology since calcite is always present in the samples, however minor morphological changes are observed indicating that slag surface has developed porosity especially CLFS 500 °C which exhibited reduction of Mg $(OH)_2$ phase. The calcination of Carbonated LFS at 1000 °C resulted in a great change of LFS morphological structure (micrograph d) by exhibiting microstructural changes associated such as alterations in grain morphology and the appearance of new crystal formations. These microstructural changes traduced by $Ca(CO)_3$ and Mg $(OH)_2$ decomposition associated with the emergence of RO phases such CaO and MgO phases have caused a great increase in specific surface area and porosity of LFS demonstrating thus the effectiveness of the modification process in producing and regenerating highly effective adsorbents.

By treating carbonated LFS with $FeSO_4/H_2O_2$ and then subjecting it to calcination at 1000 °C, notable structural alterations were observed through SEM analysis. Before alteration, the carbonated LFS showed a solid and tightly packed structure with no pores. After further analysis, SEM images show the development of pores in the material, along with the existence of highly porous and filamentous structures. The observed porosity indicates that the modification process may have caused structural changes, possibly by breaking down certain components or creating new phases during calcination. $CaSO_4$ and MgO were found in the modified material, suggesting chemical changes occurred during the modification process. $CaSO_4$ and MgO are formed due to reactions between the LFS components and $FeSO_4/H_2O_2$, followed by their decomposition and rearrangement during calcination. In addition, the thread-like structures seen in the altered material could suggest the development of crystalline phases or the reorganization of existing phases, which might be responsible for the porosity observed. These structural changes play a vital role in determining the material's characteristics and its applicability in different fields like construction materials or environmental applications.

Treatment of carbonated LFS using zinc sulphate solution

The synthesis of zinc oxide (ZnO) in a basic medium occurs easily due to the presence of hydroxide ions (OH^-), which initially promote the formation of zinc hydroxide, a compound that is thermodynamically unstable. With an increase in temperature, zinc hydroxide dehydrates to form ZnO:

$$Zn^{2+} + 2OH^- \rightarrow Zn(OH)_2$$

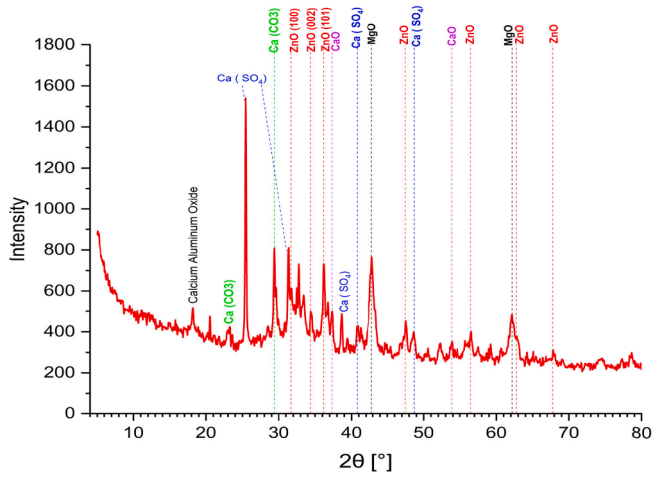

Fig. 17. XRD of the carbonated LFS modified with $ZnSO_4$.

$$Zn(OH)_2 \xrightarrow{T\uparrow} ZnO + H_2O$$

Furthermore, in our environment, the formation of ZnO can also occur through the thermal decomposition of zinc sulfate ($ZnSO_4$) at a temperature of 700 °C. This process is a compelling chemical reaction where the elevated temperature leads to the breakdown of zinc sulfate, liberating sulphate (SO_4) and facilitating the generation of zinc oxide:

$$ZnSO_4 \xrightarrow{700^\circ C} ZnO + CaSO_4$$

The alkaline environment plays a pivotal role in this synthesis by creating conducive reaction conditions. In the presence of a base, ZnO is not only favorably formed but also stabilized, promoting its crystallization. X-ray diffraction analysis (Fig. 17) provides intricate insights, showcasing the distinctive peaks associated with hexagonal Wurtzite-structured ZnO (space group P63mc). Specifically, the (1 0 0), (0 0 2), and (1 0 1) planes manifest at 2 theta angles of 31.8°, 34.4°, and 36.3°, respectively.

Additionally, the high-temperature reaction yields ZnO particles with nanometric dimensions, as illustrated in the scanning electron microscopy (Fig. 18). The nanoscale size of the ZnO particles is of paramount significance, particularly in catalytic applications, where increased surface area and unique electronic properties contribute to enhanced catalytic performance.

Conclusion

This study makes significant strides in advancing the understanding and application of carbonating metallurgical slags, particularly Ladle Furnace Slag (LFS), for sustainable waste management and resource utilization. Through meticulous examination of LFS using various analytical techniques such as X-ray Diffraction (XRD), X-ray Fluorescence (XRF), Inductively Coupled Plasma Optical Emission Spectroscopy (ICP-OES), Brunauer-Emmett-Teller (BET) analysis, and Scanning Electron Microscopy (SEM), the study underscores the remarkable adsorption capacity of LFS for Methyl Orange (MO). The kinetics of the adsorption process follow a pseudo-second-order model, with equilibrium described by the Langmuir isotherm, revealing the high adsorption capacity of LFS (Qm = 149.25 mg/g), primarily driven by chemical and electrostatic interactions.

Moreover, the investigation extends beyond mere adsorption dynamics to delve into the carbonation process itself, shedding light on the mechanisms underlying both adsorption and carbonation within LFS. This comprehensive understanding lays the groundwork for the development of innovative approaches to harness the potential of LFS in various industrial applications, including wastewater treatment, construction materials, CO_2 sequestration, and beyond.

Furthermore, the study explores avenues for enhancing the reusability of LFS-MO composites through chemical and thermal modifications. Impregnation of carbonated LFS with KOH under pyrolysis shows promise for regenerating $Ca(OH)_2$ phases responsible for MO degradation. Thermal modification at varying temperatures demonstrates significant alterations in the structure of carbonated LFS, with thermal treatment at 300 and 500 °C enhancing thermal stability and calcination at 1000 °C inducing the formation of interconnected pore networks. Additionally, the modification of carbonated LFS with $ZnSO_4$ successfully promotes the synthesis of ZnO nanoxides on the LFS surface, further expanding its potential applications.

These findings not only contribute to the sustainability of industrial processes but also offer practical solutions to address environmental challenges associated with metallurgical slags and organic dye contaminants. In essence, this study introduces a novel and holistic method for carbonating metallurgical slags, paving the way for the adoption of sustainable practices in waste management and resource utilization. Continued research and development in this area hold promise for further enhancing the efficiency, effectiveness, and scalability of carbonation techniques, ultimately contributing to the broader goals of environmental stewardship and industrial sustainability.

CRediT authorship contribution statement

Otmane Sarti: Writing – review & editing, Writing – original draft, Visualization, Software, Methodology, Investigation, Data curation, Conceptualization. **Emilia Otal:** Writing – review & editing, Writing – original draft, Visualization, Resources, Investigation. **Fouad El Mansouri:** Software, Project administration, Funding acquisition. **Hajar Ghannam:** Writing – original draft, Software, Methodology, Investigation, Formal analysis. **Salaheddine Elmoutez:** Writing – review & editing, Writing – original draft, Software, Investigation. **Mustapha El**

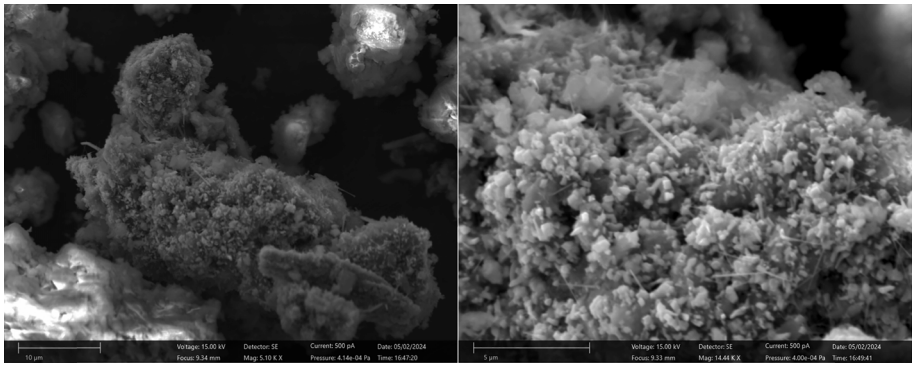

Fig. 18. Morphological characterization of Carbonated LFS treated $ZnSO_4$ at 700 °C.

Hadri: Visualization, Validation, Supervision, Formal analysis, Conceptualization. **Mohamed Saidi:** Visualization, Validation, Supervision, Project administration, Funding acquisition, Conceptualization. **José Morillo:** Visualization, Validation, Supervision, Project administration, Investigation, Formal analysis.

Declaration of competing interest

The authors declare that they have no known competing financial interests or personal relationships that could have appeared to influence the work reported in this paper.

Acknowledgements

None.

References

Abdelaziz, M.A., Owda, M.E., Abouzeid, R.E., Alaysuy, O., Mohamed, E.I., 2023. Kinetics, isotherms, and mechanism of removing cationic and anionic dyes from aqueous solutions using chitosan/magnetite/silver nanoparticles. Int. J. Biol. Macromol. 225, 1462–1475. https://doi.org/10.1016/j.ijbiomac.2022.11.203.

Albeladi, N., Kur, A., Mokaya, R., Darkwa, J., Roger-Lund, S., Worall, M., Calautit, J., Boukhanouf, R., 2023. Synthesis and Characterization of Doped Magnesium Hydroxide for Medium Heat Storage Application. Materials 16, 6296.

Ali, H., 2010. Biodegradation of Synthetic Dyes—A Review. Water Air Soil Pollut. 213, 251–273. https://doi.org/10.1007/s11270-010-0382-4.

Angın, D., Köse, T.E., Selengil, U., 2013. Production and characterization of activated carbon prepared from safflower seed cake biochar and its ability to absorb reactive dyestuff. Appl. Surf. Sci. 280, 705–710.

Arora, S., 2014. Textile Dyes: It's Impact on Environment and its Treatment. J. Bioremed. Biodegr. 05 https://doi.org/10.4172/2155-6199.1000e146.

Asaoka, S., Okamura, H., Morisawa, R., Murakami, H., Fukushi, K., Okajima, T., Katayama, M., Inada, Y., Yogi, C., Ohta, T., 2013. Removal of hydrogen sulfide using carbonated steel slag. Chem. Eng. J. 228, 843–849. https://doi.org/10.1016/j.cej.2013.05.065.

Ballotin, F.C., Santos, W.O., Mattiello, E.M., Carmignano, O., Teixeira, A.P.C., Lago, R. M., 2020. Potential slow release fertilizers based on K 2 MgSiO 4 obtained from serpentinite. J. Braz. Chem. Soc. 31, 653–661.

Bejarano-Peña, W.-D., Alcántar-Vázquez, B., Ramírez-Zamora, R.-M., 2021. Synthesis and evaluation in the CO2 capture process of potassium-modified lithium silicates produced from steel metallurgical slags. Mater. Res. Bull. 141, 111353.

Borges Marinho, A.L., Mol Santos, C.M., de Carvalho, J.M.F., Mendes, J.C., Brigolini, G. J., Peixoto, A.F., 2017. Ladle Furnace Slag as Binder for Cement-Based Composites. J. Mater. Civ. Eng. 29 https://doi.org/10.1061/(ASCE)MT.1943-5533.0002061.

Bulut, E., Özacar, M., Şengil, İ.A., 2008. Equilibrium and kinetic data and process design for adsorption of Congo Red onto bentonite. J. Hazard. Mater. 154, 613–622.

Cha, W., Kim, J., Choi, H., 2006. Evaluation of steel slag for organic and inorganic removals in soil aquifer treatment. Water Res. 40, 1034–1042. https://doi.org/10.1016/j.watres.2005.12.039.

Chung, K.-T., 2016. Azo dyes and human health: A review. J. Environ. Sci. Health C 34, 233–261.

Dong, Q., Wang, G., Chen, X., Tan, J., Gu, X., 2021. Recycling of steel slag aggregate in portland cement concrete: An overview. J. Clean. Prod. 282, 124447.

Dutta, S., Adhikary, S., Bhattacharya, S., Roy, D., Chatterjee, S., Chakraborty, A., Banerjee, D., Ganguly, A., Nanda, S., Rajak, P., 2024. Contamination of textile dyes in aquatic environment: Adverse impacts on aquatic ecosystem and human health, and its management using bioremediation. J. Environ. Manage. 353, 120103.

Eisinas, A., Dambrauskas, T., Baltakys, K., Ruginyte, K., 2019. The peculiarities of mayenite formation from synthetic katoite and calcium monocarboaluminate samples in temperature range 25–1150 °C. J. Therm. Anal. Calorim. 138, 2275–2282. https://doi.org/10.1007/s10973-019-08482-4.

Eisinas, A., Ruginyte, K., Baltakys, K., Demcak, S., Dambrauskas, T., Balintova, M., Stevulova, N., 2020. Cu2+ ion adsorption by synthetic mayenite and its thermal stability. Ceram. Int. 46, 29429–29435. https://doi.org/10.1016/j.ceramint.2020.05.028.

El-Habacha, M., Lagdali, S., Dabagh, A., Mahmoudy, G., Assouani, A., Benjelloun, M., Miyah, Y., Iaich, S., Chiban, M., Zerbet, M., 2024. High efficiency of treated-phengite clay by sodium hydroxide for the Congo red dye adsorption: optimization, cost estimation, and mechanism study. Environ. Res. 119542 https://doi.org/10.1016/j.envres.2024.119542.

Fang, Y., Shan, J., Wang, Q., Zhao, M., Sun, X., 2024. Semi-dry and aqueous carbonation of steel slag: Characteristics and properties of steel slag as supplementary cementitious materials. Constr. Build. Mater. 425, 135981.

Gomari, K.E., Gomari, S.R., Hughes, D., Ahmed, T., 2024. Exploring the potential of steel slag waste for carbon sequestration through mineral carbonation: A comparative study of blast-furnace slag and ladle slag. J. Environ. Manage. 351, 119835.

Haque, M.M., Haque, M.A., Mosharaf, M.K., Marcus, P.K., 2021. Decolorization, degradation and detoxification of carcinogenic sulfonated azo dye methyl orange by newly developed biofilm consortia. Saudi J. Biol. Sci. 28, 793–804.

Hu, Z.-P., Gao, Z.-M., Liu, X., Yuan, Z.-Y., 2018. High-surface-area activated red mud for efficient removal of methylene blue from wastewater. Adsorpt. Sci. Technol. 36, 62–79.

Huang, X., Zhang, J., Zhang, L., 2024. Accelerated carbonation of steel slag: A review of methods, mechanisms and influencing factors. Constr. Build. Mater. 411, 134603.

Huijgen, W.J.J., Comans, R.N.J., 2006. Carbonation of steel slag for CO2 sequestration: leaching of products and reaction mechanisms. Environ. Sci. Tech. 40, 2790–2796.

Humbert, P.S., Castro-Gomes, J., 2019. CO2 activated steel slag-based materials: A review. J. Clean. Prod. 208, 448–457. https://doi.org/10.1016/j.jclepro.2018.10.058.

Jebli, A., Amri, A.E., Hsissou, R., Lebkiri, A., Zarrik, B., Bouhassane, F.Z., Hbaiz mahdi, E., Rifi, E.H., Lebkiri, Ahmed, 2023. Synthesis of a chitosan@hydroxyapatite composite hybrid using a new approach for high-performance removal of crystal violet dye in aqueous solution, equilibrium isotherms and process optimization. J. Taiwan Inst. Chem. Eng. 149, 105006 https://doi.org/10.1016/j.jtice.2023.105006.

Ji, R., Liu, T.-J., Kang, L.-L., Wang, Y.-T., Li, J.-G., Wang, F.-P., Yu, Q., Wang, X.-M., Liu, H., Guo, H.-W., Xu, W.-L., Zeng, Y.-N., Fang, Z., 2022. A review of metallurgical slag for efficient wastewater treatment: Pretreatment, performance and mechanism. J. Clean. Prod. 380, 135076 https://doi.org/10.1016/j.jclepro.2022.135076.

Jiang, Y., Ling, T.-C., Shi, C., Pan, S.-Y., 2018. Characteristics of steel slags and their use in cement and concrete—A review. Resour. Conserv. Recycl. 136, 187–197.

Kim, K., Nakashita, S., Yoshimura, K., Hibino, T., 2021. In situ electrochemical remediation of brackish river sediment rich in aromatic organic matter using steel-slag-combined sediment microbial fuel cells. J. Clean. Prod. 315, 128206 https://doi.org/10.1016/j.jclepro.2021.128206.

Kishor, R., Saratale, G.D., Saratale, R.G., Ferreira, L.F.R., Bilal, M., Iqbal, H.M.N., Bharagava, R.N., 2021. Efficient degradation and detoxification of methylene blue dye by a newly isolated ligninolytic enzyme producing bacterium Bacillus albus MW407057. Colloids Surf. B Biointerfaces 206, 111947.

Lebkiri, I., Abbou, B., Hsissou, R., Safi, Z., Sadiku, M., Berisha, A., El Amri, A., Essaadaoui, Y., Kadiri, L., Lebkiri, A., Rifi, E.H., 2023. Investigation of the anionic polyacrylamide as a potential adsorbent of crystal violet dye from aqueous solution: Equilibrium, kinetic, thermodynamic, DFT, MC and MD approaches. J. Mol. Liq. 372, 121220 https://doi.org/10.1016/j.molliq.2023.121220.

Lin, J., Zhan, Y., 2012. Adsorption of humic acid from aqueous solution onto unmodified and surfactant-modified chitosan/zeolite composites. Chem. Eng. J. 200–202, 202–213. https://doi.org/10.1016/j.cej.2012.06.039.

Liu, J., Wang, D., 2017. Influence of steel slag-silica fume composite mineral admixture on the properties of concrete. Powder Technol. 320, 230–238. https://doi.org/10.1016/j.powtec.2017.07.052.

Loutfi, M., Mariouch, R., Mariouch, I., Belfaquir, M., ElYoubi, M.S., 2023. Adsorption of methylene blue dye from aqueous solutions onto natural clay: Equilibrium and kinetic studies. Mater. Today:. Proc. 72, 3638–3643. https://doi.org/10.1016/j.matpr.2022.08.412.

Maruthanayagam, A., Mani, P., Kaliappan, K., Chinnappan, S., 2020. In vitro and in silico studies on the removal of methyl orange from aqueous solution using Oedogonium subplagiostomum AP1. Water Air Soil Pollut. 231, 1–21.

Naidu, T.S., Sheridan, C.M., van Dyk, L.D., 2020. Basic oxygen furnace slag: Review of current and potential uses. Miner. Eng. 149, 106234 https://doi.org/10.1016/j.mineng.2020.106234.

Nidheesh, P.V., Zhou, M., Oturan, M.A., 2018. An overview on the removal of synthetic dyes from water by electrochemical advanced oxidation processes. Chemosphere 197, 210–227. https://doi.org/10.1016/j.chemosphere.2017.12.195.

Rađenović, A., Malina, J., Sofilić, T., 2013. Characterization of ladle furnace slag from carbon steel production as a potential adsorbent. Adv. Mater. Sci. Eng. 2013, 1–6.

Rovnushkin, V.A., Visloguzova, E.A., Spirin, S.A., Shekhovtsov, E.V., Kromm, V.V., Metelkin, A.A., 2005. Composition of ladle slag and refractory materials and its effect on the wear resistance of the lining of an RH vacuum degasser. Refract. Ind. Ceram 46, 193–196.

Saoud, K.M., Saeed, S., Al-Soubaihi, R.M., Bertino, M.F., 2014. Microwave assisted preparation of magnesium hydroxide nano-sheets. Am. J. Nanomater. 2, 21–25.

Sarti, O., El Mansouri, F., Yahia, E.H., Otal, E., Morillo, J., Saidi, M., 2023. Efficient Removal of Tannic Acid from Olive Mill Wastewater Using Carbon Steel Slag. C 9, 32. https://doi.org/10.3390/c9010032.

Setién, J., Hernández, D., González, J.J., 2009. Characterization of ladle furnace basic slag for use as a construction material. Constr. Build. Mater. 23, 1788–1794.

Suteu, D., Bilba, D., 2005. Equilibrium and kinetic study of reactive dye Brilliant Red HE-3B adsorption by activated charcoal. Acta Chim. Slov 52, 73–79.

Temkin, M.I., 1940. Kinetics of ammonia synthesis on promoted iron catalysts. Acta Physiochim. URSS 12, 327–356.

Tkaczyk, A., Mitrowska, K., Posyniak, A., 2020. Synthetic organic dyes as contaminants of the aquatic environment and their implications for ecosystems: A review. Sci. Total Environ. 717, 137222 https://doi.org/10.1016/j.scitotenv.2020.137222.

Tsai, T.T., Kao, C.M., 2009. Treatment of petroleum-hydrocarbon contaminated soils using hydrogen peroxide oxidation catalyzed by waste basic oxygen furnace slag. J. Hazard. Mater. 170, 466–472. https://doi.org/10.1016/j.jhazmat.2009.04.073.

Wang, M., Lan, X., Xu, X., Fang, Y., Singh, B.P., Sardans, J., Romero, E., Peñuelas, J., Wang, W., 2020. Steel slag and biochar amendments decreased CO2 emissions by altering soil chemical properties and bacterial community structure over two-year in a subtropical paddy field. Sci. Total Environ. 740, 140403 https://doi.org/10.1016/j.scitotenv.2020.140403.

Wang, Z., Song, B., Li, J., Teng, X., 2021b. Degradation of norfloxacin wastewater using kaolin/steel slag particle electrodes: Performance, mechanism and pathway. Chemosphere 270, 128652. https://doi.org/10.1016/j.chemosphere.2020.128652.

Wang, S., Yao, S., Du, K., Yuan, R., Chen, H., Wang, F., Zhou, B., 2021a. The mechanisms of conventional pollutants adsorption by modified granular steel slag. Environ. Eng. Res. 26.

Wang, D., Zhang, H., Liu, M., Fu, Y., Si, Z., Zhang, X., Zhong, Q., 2023. The characterization and mechanism of carbonated steel slag and its products under low CO2 pressure. Mater. Today Commun. 35, 105827 https://doi.org/10.1016/j.mtcomm.2023.105827.

Xu, B., Yi, Y., 2022. Treatment of ladle furnace slag by carbonation: Carbon dioxide sequestration, heavy metal immobilization, and strength enhancement. Chemosphere 287, 132274. https://doi.org/10.1016/j.chemosphere.2021.132274.

Yi, H., Xu, G., Cheng, H., Wang, J., Wan, Y., Chen, H., 2012. An Overview of Utilization of Steel Slag. Procedia Environ. Sci. 16, 791–801. https://doi.org/10.1016/j.proenv.2012.10.108.

Yildirim, I.Z., Prezzi, M., 2011. Chemical, mineralogical, and morphological properties of steel slag. Advances in civil engineering 2011.

Zavahir, S., Elmakki, T., Ismail, N., Gulied, M., Park, H., Han, D.S., 2023. Degradation of Organic Methyl Orange (MO) Dye Using a Photocatalyzed Non-Ferrous Fenton Reaction. Nanomaterials 13, 639. https://doi.org/10.3390/nano13040639.

Zhang, Z., Feng, Y., Liu, N., Zhao, Y., Wang, X., Yang, S., Long, Y., Qiu, L., 2020. Preparation of Sn/Mn loaded steel slag zeolite particle electrode and its removal effect on rhodamine B (RhB). J. Water Process Eng. 37, 101417.

Zhang, Y., Ying, Y., Xing, L., Zhan, G., Deng, Y., Chen, Z., Li, J., 2024. Carbon dioxide reduction through mineral carbonation by steel slag. J. Environ. Sci.